ARL-TR-8629 ● JAN 2019

US Army Research Laboratory

A Mechanochemistry-Based Technique for Early Material Damage Detection in High Strain Rate Processes

by Logan Shannahan, James Berry, Yangju Lin, Meredith Barbee, Stephen Craig, Daniel Casem, and Müge Fermen-Coker

NOTICES

Disclaimers

The findings in this report are not to be construed as an official Department of the Army position unless so designated by other authorized documents.

Citation of manufacturer's or trade names does not constitute an official endorsement or approval of the use thereof.

Destroy this report when it is no longer needed. Do not return it to the originator.

ARL-TR-8629 ● JAN 2019

US Army Research Laboratory

A Mechanochemistry-Based Technique for Early Material Damage Detection in High Strain Rate Processes

by Logan Shannahan, Daniel Casem, and Müge Fermen-Coker
Weapons and Materials Research Directorate, ARL

James Berry
SURVICE Engineering, Belcamp, MD

Yangju Lin, Meredith Barbee, and Stephen Craig
Duke University, Durham, NC

REPORT DOCUMENTATION PAGE

Form Approved
OMB No. 0704-0188

1. REPORT DATE *(DD-MM-YYYY)*	2. REPORT TYPE	3. DATES COVERED (From - To)
January 2019	Technical Report	October 2017–September 2018

4. TITLE AND SUBTITLE
A Mechanochemistry-Based Technique for Early Material Damage Detection in High Strain Rate Processes

5a. CONTRACT NUMBER

5b. GRANT NUMBER

5c. PROGRAM ELEMENT NUMBER

6. AUTHOR(S)
Logan Shannahan, James Berry, Yangju Lin, Meredith Barbee, Stephen Craig, Daniel Casem, and Müge Fermen-Coker

5d. PROJECT NUMBER

5e. TASK NUMBER

5f. WORK UNIT NUMBER

7. PERFORMING ORGANIZATION NAME(S) AND ADDRESS(ES)
US Army Research Laboratory
ATTN: RDRL-WMP-C
Aberdeen Proving Ground, MD 21005-5069

8. PERFORMING ORGANIZATION REPORT NUMBER
ARL-TR-8629

9. SPONSORING/MONITORING AGENCY NAME(S) AND ADDRESS(ES)

10. SPONSOR/MONITOR'S ACRONYM(S)

11. SPONSOR/MONITOR'S REPORT NUMBER(S)

12. DISTRIBUTION/AVAILABILITY STATEMENT
Approved for public release; distribution is unlimited.

13. SUPPLEMENTARY NOTES
This report has been edited per the style guide *Scientific Style and Format: The CSE Manual for Authors, Editors, and Publishers.* 8th ed. Chicago (IL): University of Chicago Press; 2014.

14. ABSTRACT
It is often desired to detect damage at the sub-continuum level before continuum-level damage is observed. The burgeoning field of polymer mechanochemistry promises development of novel materials that would report sub-continuum-level damage if a critical stress or strain level is exceeded. In addition, a long-standing challenge for multi-scale modeling validation has been the generation of experimental data to link molecular-level damage to macroscopic material behavior at high rate. Using mechanophore-embedded silicone elastomer samples, for the first time ever, molecular-level bond breakage is captured visually during standard high-rate material characterization experiments, prior to the onset of macroscopic damage. A brief description of synthesized mechanophores, methods of embedding into the silicone elastomer, and the method to determine the critical strain of mechanophore activation (molecular-level bond breakage) is included. The critical strain and critical stress values are determined for the onset of molecular-level bond breakage. Constitutive models enhanced with the method presented in this report can potentially be used for validation of multi-scale material failure computational model development efforts to simulate ballistic impact events. The results reported herein contribute to the investigations of mechanophore-embedded materials for enhanced stress assessment and for the development of mechanophore-based adaptive/multifunctional protection materials.

15. SUBJECT TERMS
mechanochemistry, mechanophore, Split Hopkinson Pressure Bar, SPHB, Kolsky, high-rate material behavior, multi-scale model validation, organic synthesis

16. SECURITY CLASSIFICATION OF:			17. LIMITATION OF ABSTRACT	18. NUMBER OF PAGES	19a. NAME OF RESPONSIBLE PERSON
a. REPORT	b. ABSTRACT	c. THIS PAGE			Müge Fermen-Coker
Unclassified	Unclassified	Unclassified	UU	37	19b. TELEPHONE NUMBER (Include area code) 410-278-6018

Standard Form 298 (Rev. 8/98)
Prescribed by ANSI Std. Z39.18

Contents

List of Figures

List of Tables

Acknowledgments

The authors acknowledge the support of the US Army Research Laboratory's Weapons and Materials Research Directorate for this work. The mold used for cast curing silicone elastomer samples as displayed in Fig. 5 of this report was designed by Travis Neidenfeuhr.

1. Motivation

Recent advances in materials science and chemistry present new opportunities to develop improved and novel protection mechanisms. One of the exciting areas is mechanochemistry—the study of mechanically driven chemistry (i.e., the coupling between macroscopic mechanical loads and chemical reactivity). When mechanophores (force-sensitive chemical species) are embedded into materials, mechanical force can be used to drive chemical reactivity. The activation and outcome of the chemical reaction due to mechanical loading can be tailored to "change" or "adapt" the continuum-level mechanical properties and, therefore, the response. Adaptive responses made possible through the use of mechanophores can be explored to achieve previously unattainable options and performance from material systems. Various potential applications can be made possible once our understanding of such systems is improved to the level of properly manipulating them, as well as integrating them into designed/engineered features in protection systems to improve the technologies available for protection of the Soldier.

The objective of the current research effort at the US Army Research Laboratory, in collaboration with Duke University, is to synthesize mechanophores and manufacture materials with embedded mechanophores to understand, verify, validate, characterize, and tailor ballistic performance of these new constructs with the ultimate goal of developing superior protection mechanisms. To achieve this objective, the following research questions need to be addressed:

- Can mechanophore activation be tailored for critical stress reporting that would be useful for monitoring or assessing Soldier health, equipment safety, and overall improved protection?
- Can useful adaptive materials or multifunctional materials be manufactured through mechanophore embedding for ballistic applications that would enhance Soldier or vehicle protection at levels that cannot be attained through existing protection materials?

As a first step toward this endeavor, the work covered in this report demonstrates a new experimental protocol that captures mechanophore activation as part of constitutive model development and also as validation data for multi-scale modeling of material failure due to high-rate loading.

2. Introduction

Many articles on mechanical activation of chemical bonds have appeared in print during the last three decades. An excellent review by Beyer and Clausen-Schaumann[1] points out that the first written document mentioning a mechanochemical reaction can date as far back as 371–286 BC. This review also mentions that there has been groundbreaking research on polymers during the 1940s to establish a stronger basis for further research on the topic. In fact, institutes and international associations have been formed on the subject of mechanochemistry since the 1990s. The field of polymer mechanochemistry has further burgeoned in the past decade, with advances including self-healing materials,[2] soft robots,[3] devices,[4] electronics[5] and 3-D printed materials.[6]

The ability to take a process historically viewed as destructive, such as the scission of a polymer chain, and turn it into a constructive outcome is the hallmark of this intersection of chemistry and materials science.[7,8] Polymer mechanochemistry is centered around the use of mechanophores.[7] When incorporated into a polymer chain and subjected to external force, tensile force builds along the chain to stress the weak bond of the mechanophore.[9] For fundamental studies using sonication, mechanophores are typically found at or near the center of the polymer chain, where maximal stress accumulates.[8] Mechanophores have been produced that can undergo color change,[10] react with other molecules in the nearby medium,[11] release small molecules,[12,13] and generate acid[14] or active catalysts.[15]

Covalent bonds are stretched in the presence of an external mechanical force. Destructive loading can cause bond scission and further failure in synthetic polymers. Alternatively, these destructive forces can be channeled into constructive, localized, bond-forming reactions. Realization of useful reaction outcomes through destructive mechanical loading is made possible through the use of mechanophores.

In terminal ballistics, computational studies are conducted to predict the outcome of ballistic impact events involving various penetrators against target materials. Penetrator and target material behaviors are characterized under dynamic loading and the resulting material models are incorporated into computational codes.

One of the standard material characterization techniques involves the use of Split Hopkinson Pressure Bar (SHPB), also known as the Kolsky bar. Most research efforts involving failure of mechanophore-embedded materials under mechanical loading have been associated with quasi-static or low strain rate loading. Celestine et al. investigated the fracture behavior of mechanophore-linked glassy polymers.[16] They incorporated spiropyran (SP) into poly(methyl methacrylate) (PMMA) and

explored the fracture behavior of linear and cross-linked spiropyran-embedded PMMA. Grady et al. detected activation of a spiropyran-embedded glassy polystyrene coating under high strain rates using shockwaves, while no activation was observed for the same material under quasi-static loading.[17]

Kingsbury et al. investigated shear loading on bulk polymer specimens of PMMA embedded with spiropyran mechanophores that undergo an electrocyclic ring-opening reaction that transforms a colorless nonfluorescent molecule into its merocyanine form, which is a highly colored and fluorescent molecule.[18] This reaction is reversible and can occur due to mechanical force, exposure to certain wavelengths of light, as well as through heat.

There has been at least one Kolsky bar experiment reported in literature involving mechanophore-embedded materials prior to our effort. Hemmer et al.[19] investigated SP mechanophores in PMMA using a Kolsky bar at rates between 10^2 and 10^4/s. They observed macro-level damage in their specimens, where spiropyran activation was significant near fracture surfaces. They attributed much of the activation to thermal effects during high-rate fracture events.

The current effort reported herein is, to the best of our knowledge, the first effort that detects and quantifies the onset of mechanophore activation in elastic materials during a high strain rate event, indicating molecular-level bond breakage, linking it to macroscopic strain and stress levels, prior to macroscopic damage or fracture.

Schemes for the synthesis of two different mechanophores are included in this report. The first is a functionalized spiropyran mechanophore and the second is a control spiropyran to ensure that the activity of the functionalized spiropyran mechanophore is mechanical in nature, and not due to local thermal effects, when subjected to the same level and rate of mechanical loading. For the control series, the alkene linker groups were placed on the same side of the molecule to avoid stress accumulation at the spirocyclic center, which prevents mechanical activation to the colored merocyanine structure.

3. Mechanophore Chemistry

Various mechanophores have been synthesized to report the effect of force on a polymeric system. Molecules such as spiropyrans,[20,21] coumarin dimers,[22] diarylbibenzylfuranones,[23] naphthopyrans,[24] rotaxanes,[25] ferrocenes,[26,27] and *gem*-dihalocyclopropanes[28] have been synthesized and incorporated into polymeric systems. Spiropyrans, naphthopyrans, rotaxanes, and diarylbibenzylfuranones are mechanophores that have reversible reaction pathways, allowing them to revert back to their initial state after activation. Coumarin dimers, ferrocenes and *gem*-

dihalocyclopropanes are examples of irreversible mechanophores—those whose reaction products cannot overcome the activation energy barrier to revert back to the starting mechanophore, or are split into separate molecules that cannot recombine. Among the aforementioned molecules, spiropyrans represent an interesting class of molecules with several relevant properties that make them an ideal choice for this application. First, the transformation from spiropyran (pale yellow) to merocyanine (deep blue/purple) provides a robust contrast in color, easily demonstrating mechanophore activity (Fig. 1). Second, this spiropyran to merocyanine reaction is also reversible. Third, the structure of the spiropyran mechanophore allows for the release of stored length within the molecule, thus preventing scission of the polymer chain in bulk material. Finally, the spiropyran structure can be functionalized with groups that attach to the alcohol functionalities present on the spiropyran itself. In this case, the addition of alkene linkers will allow attachment of the spiropyran molecule directly to the backbone of polydimethylsiloxane (PDMS) during the curing process. This is important because during testing, the force experienced by the bulk PDMS can be transferred to the weak spirocyclic C-O bond (red bond, Fig. 1). These properties of functionalized spiropyrans—in particular, the contrast in color from the inactive to active form—enable visualization of molecular-level bond breakage (the spiro C-O bond; red bond Fig. 1) during continuum loading. This feature is utilized in this effort by incorporating mechanophore embedded materials into standard high-rate material characterization experiments to determine the onset of molecular-level bond breakage as part of the constitutive behavior of the material. The functionalized spiropyran **1** (Fig. 2) was chosen as the mechanophore for this study.

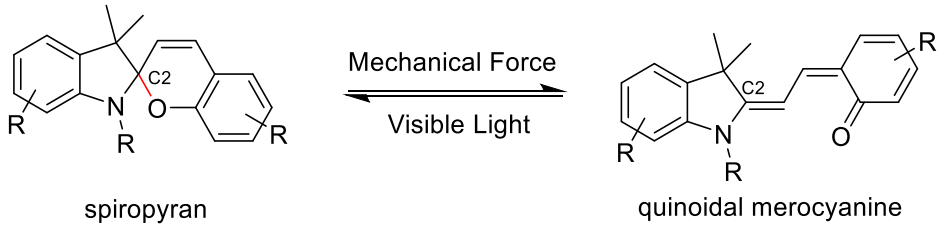

(a)

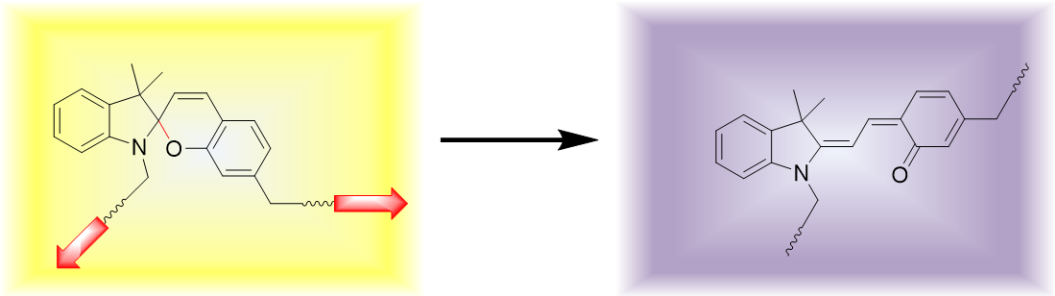

(b)

Fig. 1 (a) The spiropyran to merocyanine transition due to mechanical force. The spiro C-O bond shown in red is the weak bond that is broken during this transformation. (b) Color change from yellow to purple that takes place during this process.[7]

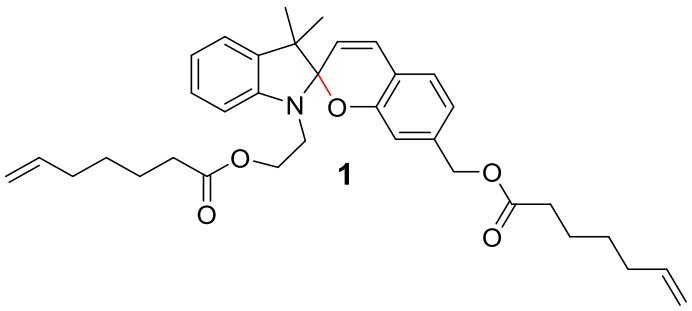

Fig. 2 Functionalized spiropyran 1 used in this study

Mechanophore studies can be performed either in solution, in which pulsed ultrasound produces cavitation bubbles,[8] or in a bulk polymer, which can be acted upon by another object. We are interested in the bulk polymer area of mechanophore activity. Davis et al.[29] reported the use of a functionalized spiropyran molecule embedded within two different polymers, the elastomeric poly(methyl acrylate), PMA, and the glassy poly(methyl methacrylate), PMMA. Building on this work, Gossweiler et al.[13] disclosed the incorporation of a slightly modified functionalized spiropyran into elastomeric PDMS, which could be activated repeatedly without loss of activity or destruction of sample material. However, both of these reports focused on quasi-static loading of the mechanophore-embedded material. Hemmer et al.[19] embedded a spiropyran

mechanophore into glassy PMMA and tested under high-rate conditions, but the sample material became damaged in the process. Our interest was to visually capture molecular-level bond breakage prior to continuum-level damage to the material. Optical transparency as well as mechanical strength were also considered in selecting the bulk material. For these reasons, PDMS was chosen as the bulk material for incorporation of functionalized mechanophore **1.**[*]

3.1 Synthesis of Functionalized Spiropyran Mechanophore

The synthesis of functionalized spiropyran **1** (see Appendix for all synthetic procedures and characterization data) used in this study was adapted from a previous work in the Craig lab.[13]The synthesis commenced with alkylation[13] of indole **2** with 2-iodoethanol in refluxing toluene to give alkylated indole **3**. Spiropyran formation[13] was accomplished through reaction of indolium iodide **3** and diol **4**[30] under basic conditions in refluxing ethanol. Finally, functionalization of spiropyran **5** through acylation[13,31] with hept-6-enoic anhydride gave mechanophore **1** (Fig. 3).[†]

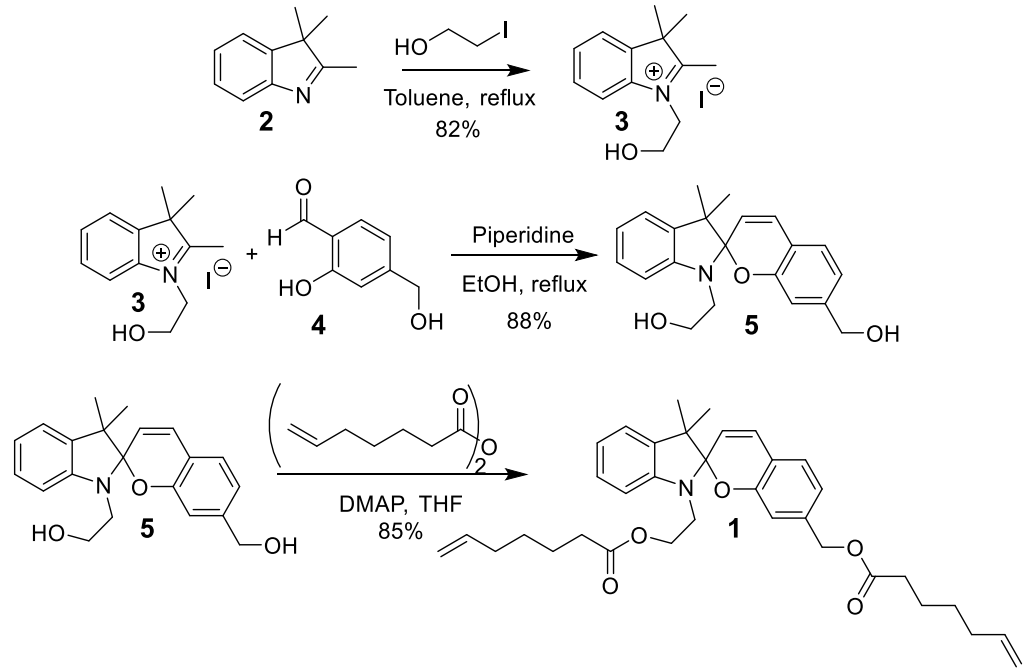

Fig. 3 Scheme 1: Synthesis of functionalized spiropyran 1

[*] The numbers in bold correspond to the numbered chemical structures in Figs. 2–4.

[†] Additional information on the workup and isolation of nitro-substituted functionalized spiropyrans without recrystallization is detailed in a separate Army Research Laboratory report (Berry JF. Facile isolation of functionalized spiropyrans without recrystallization. Aberdeen Proving Ground [MD]: Army Research Laboratory [US]; 2018 Sept. Report No.: ARL-CR-0830).

3.2 Synthesis of Control Spiropyran

To ensure that the activity of the functionalized spiropyran mechanophore was mechanical in nature, and not due to local thermal effects,[7] control spiropyran **12** was synthesized (Fig. 4). Alkene linker groups were placed on the same side of the molecule, which would avoid stress accumulation at the spirocyclic center of **12** and therefore prevent mechanical activation to the colored merocyanine molecule. This synthesis began with 4-methoxyphenylhydrazine hydrochloride **6**, which was combined with methyl isopropyl ketone under refluxing conditions to give indole **7**.[21] Deprotection of the phenol of **7** under acidic conditions gave **8,**[29] which was then alkylated with 2-iodoethanol in refluxing toluene to give alkylated indole **9**.[13] Treatment of indolium iodide **9** with commercially available 2-hydroxy-5-nitro-benzaldehyde **10** in the presence of base afforded spiropyran **11** in high yield.[29] Finally, acylation of spiropyran **11** with 4-pentenoic anhydride gave control spiropyran **12** (Fig. 4).[13]

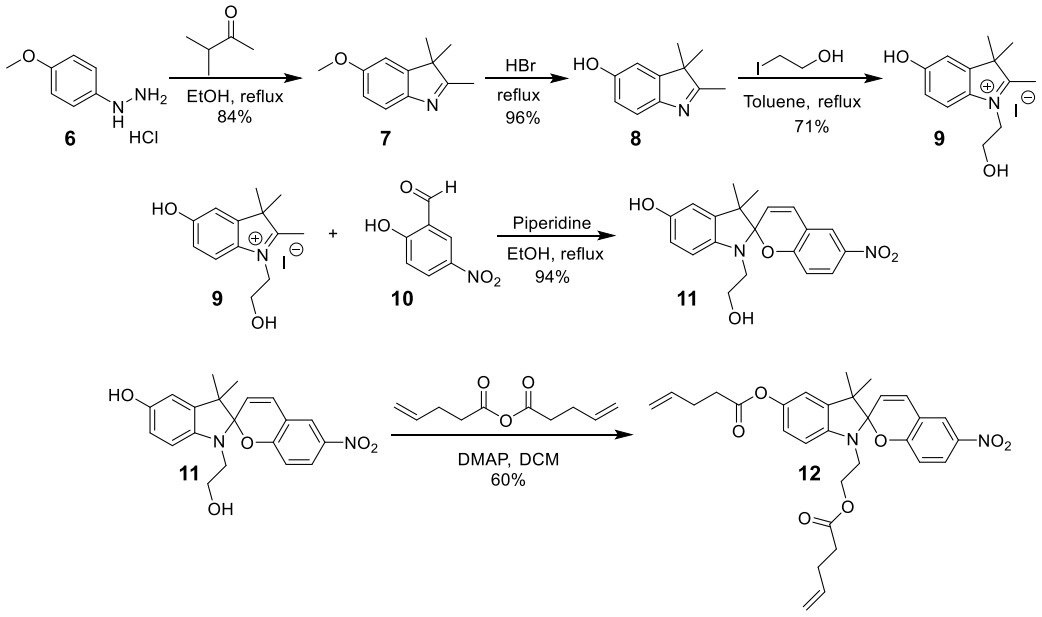

Fig. 4 Scheme 2: Synthesis of control spiropyran 12

To incorporate the functionalized spiropyran mechanophore into PDMS[13] and cast the proper-sized (0.25-inch diameter) cylindrical samples for testing, an aluminum mold (Fig. 5a and 5b) was used to cure the samples. The mold consisted of four plates, two of which were fitted together to form the main housing of the sample. The solid bottom plate was used for support and as a barrier to contain the pre-cured mixture. The entry holes on the top plate shown in Fig. 5 were used for the introduction of the mechanophore/PDMS mixture into the mold (Fig. 5a). This top portion also served as an escape for any air bubbles that formed while pouring the mixture.

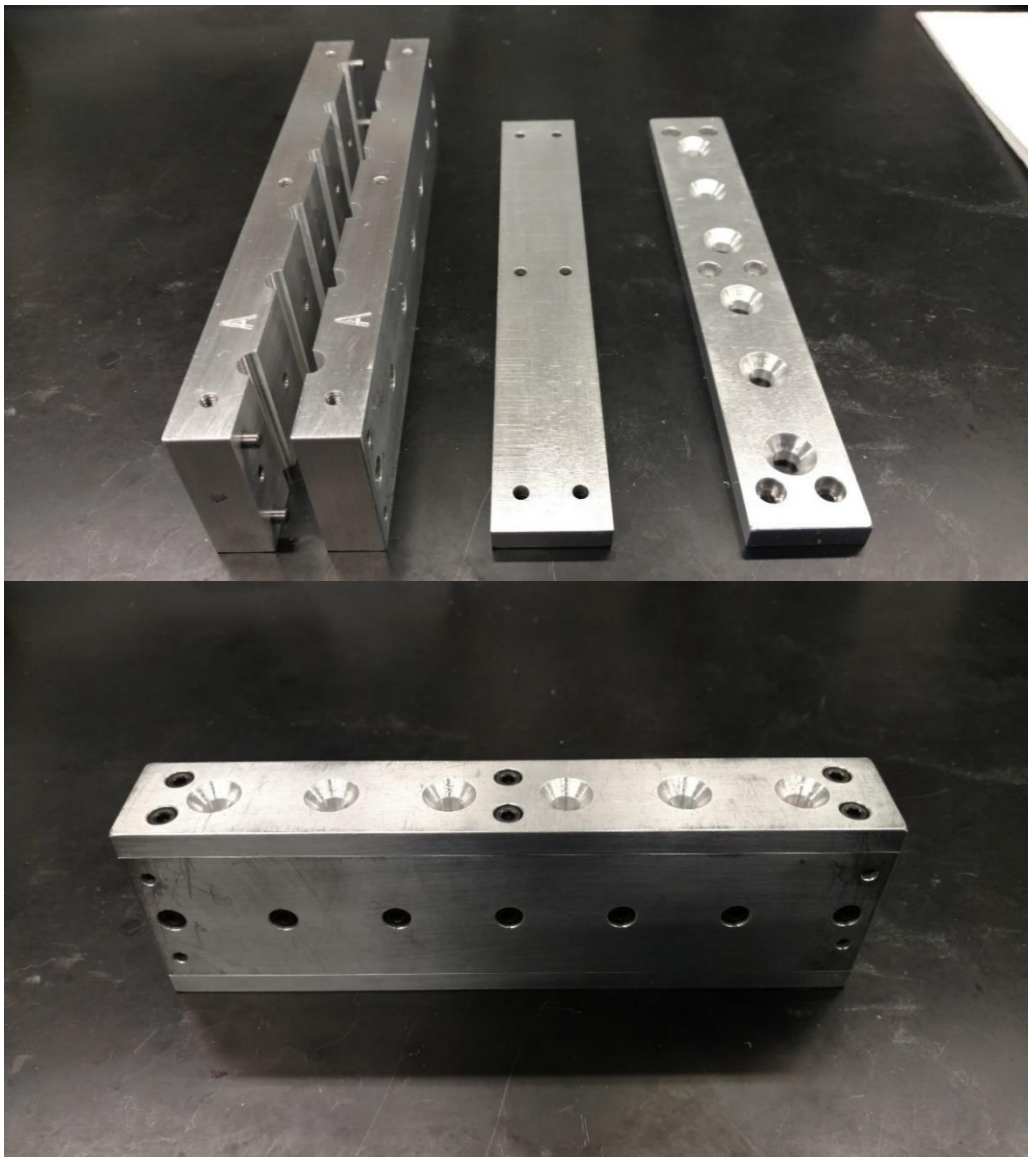

Fig. 5 Disassembled (top) and assembled (bottom) mold for casting PDMS samples

To create the samples used for ballistic impact testing, functionalized spiropyran **1** or control spiropyran **12** (0.5% by weight) in a minimal quantity (0.5 mL) of xylenes was added to the elastomer base of Sylgard 184 and vortexed. To this suspension was added the curing agent and the mixture vortexed again for proper mixing. This final suspension was poured slowly into each of the cavities of the mold, which was then placed under vacuum to remove any remaining air bubbles. After 1 h under vacuum, the mold was returned to atmospheric pressure and cured at 68 °C for 24 h. Upon cooling, the material was gently removed from the mold with the aid of a small metal spatula to obtain the requisite cylinders (0.25-inch diameter, Fig. 6). Several samples could then be cut from each cylinder using a razor blade.

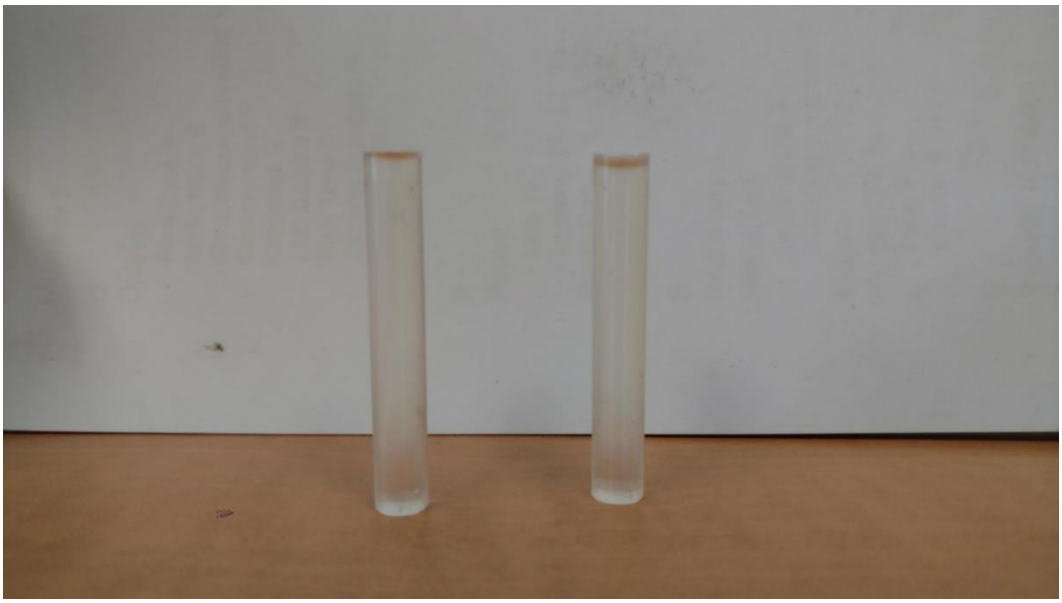

Fig. 6 Cylindrical samples from the curing process

4. High-Rate Material Characterization Experiments

In a typical Kolsky bar experiment, the sample is placed between two long bars. A coaxially aligned projectile is fired using a gas gun into the end of one bar (the "incident bar") and an elastic stress pulse generated (Fig. 7). This stress pulse travels down the incident bar, through the sample, and into the second, or "transmission" bar. Strain gauges on both bars measure the incident stress pulse, the transmitted stress pulse, and the reflected stress pulse from the sample. One-dimensional wave mechanics and knowledge of the bar mechanical properties allow calculation of the stress and strain state in the sample through the duration of the experiment.[32] Using 1-D wave mechanics, the governing equations to determine strain rate, strain, and stress ($\dot{\varepsilon}, \varepsilon,$ and σ, respectively) in a Kolsky experiment are as follows:

$$\dot{\varepsilon} = -2\frac{C_b}{L_s}\varepsilon_R \, . \tag{1}$$

$$\varepsilon = -2\frac{C_b}{L_s}\int_0^t \varepsilon_R \, dt \, . \tag{2}$$

$$\sigma = \frac{A_b}{A_s}E_b\varepsilon_T \, . \tag{3}$$

In these expressions, C_b is the elastic wave speed in the bar, L_s is the original length of the sample, A_b is the area of the bar, A_s is the original area of the sample, E_b is the elastic modulus of the bar, ε_R is the reflected pulse captured by the strain gauges, and ε_T is the transmitted pulse.

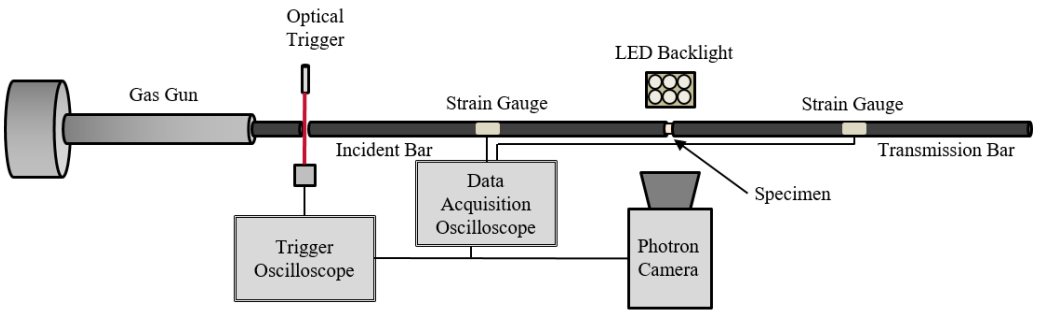

Fig. 7 Schematic of Kolsky (Split Hopkinson) bar experimental setup

Polycarbonate was chosen as the bar material as it allows for a longer input stress wave better suited for investigation of a soft, low-impedance material such as PDMS, and for improved sensitivity to the stress state in the sample. The wave speed of the polycarbonate used in this study was found experimentally to be 1821 m/s. The diameter of the bars was 12.4 mm. The striker was made of polycarbonate as well, with a length of 0.5 m and a diameter of 9.5 mm. The PDMS samples had a nominal diameter of 9.5 mm and a length of 5 mm. All experiments in this study were carried out at a consistent firing pressure of 30 psi. The ends of the bars were greased with mineral oil to reduce friction on the bar-sample interface and to reduce barreling of the sample. Sample equilibrium was examined during analysis for each experiment and confirmed valid.

While beneficial for the study of soft materials, the use of polycarbonate as a bar material introduces both significant dispersion effects and viscoelastic effects in the waveform transmitted by the bars. For the assumptions used in analysis of Kolsky data to hold, it is necessary to compensate for these effects. In this case, the method developed by Bacon based on bar radial inertia and material properties was used.[33] First, the damping coefficient as a function of frequency a(ω) and the phase velocity as a function of frequency c(ω) are determined from analyzing a single pulse measured at two positions on the same bar, or as in this case, measuring a single pulse during transmission down the bar and again after reflection off the free end of the bar. The Fourier transform of both signals is taken, and a(ω) found as follows:

$$\mathrm{a}(\omega) = Real\left[-\frac{1}{x}\ln\left(\frac{\tilde{\varepsilon}_2}{\tilde{\varepsilon}_1}\right)\right], \tag{4}$$

where $\tilde{\varepsilon}_1$ is the Fourier transform of the first measured strain pulse, $\tilde{\varepsilon}_2$ is the Fourier transform of the second measured strain pulse, and x is the distance between the gauges used to measure the strain pulses. The phase velocity c(ω) is found in a similar fashion:

$$\mathrm{c}(\omega) = \frac{\omega \mathrm{x}}{p_2 - p_1}, \tag{5}$$

in which ω is the angular frequency and p_2 and p_1 are the phase angles of $\tilde{\varepsilon}_2$ and $\tilde{\varepsilon}_1$, respectively. Using these coefficients, a general solution for the corrected Fourier transform of the strain signal at an arbitrary location along the bar x is given as

$$\tilde{\varepsilon}(x,\omega) = \tilde{P}(\omega)e^{-\gamma x}, \tag{6}$$

where $\tilde{P}(\omega)$ is the Fourier transform of the strain signal at the incident strain gauge and γ is the propagation coefficient, defined by the following expression:

$$\gamma(\omega) = a(\omega) + i\frac{\omega}{c(\omega)}. \tag{7}$$

This correction method is demonstrated in Fig. 8, where an initial pulse is corrected and compared to a second measured pulse with close agreement, suggesting the correction is accurate. In an actual experiment, the pulse recorded by the strain gauge is corrected to the location of the sample using the above expressions, rather than simply shifting the measured pulse in time as in a typical Kolsky experiment using elastic bars.

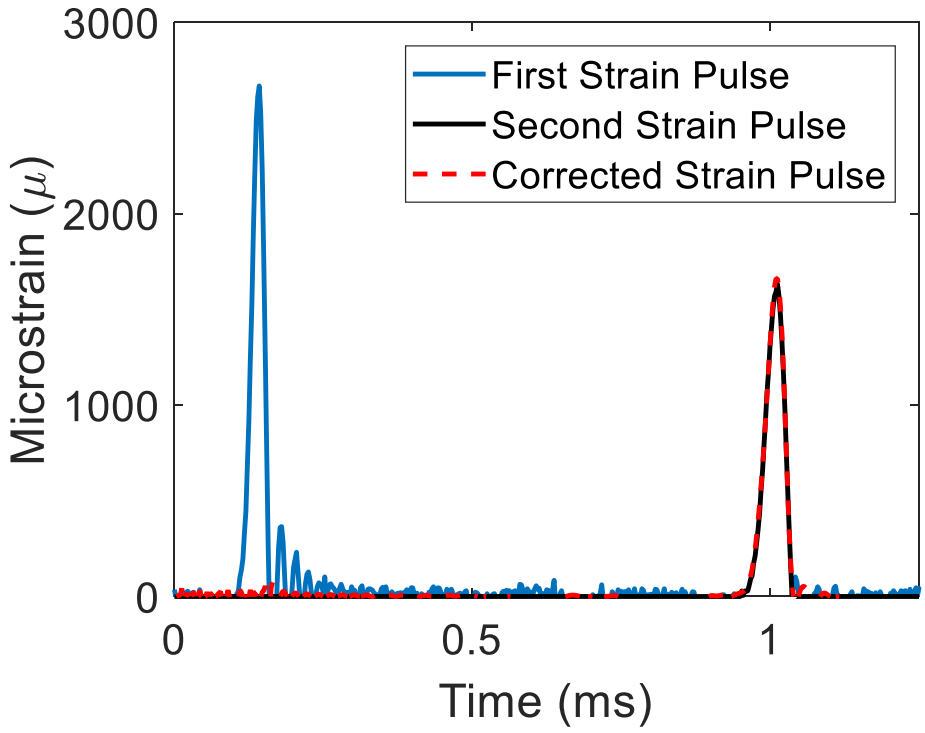

Fig. 8 The viscoelastic correction is verified by comparing the second measured strain pulse (black) to the corrected pulse (red) derived from the initial pulse (blue). The difference in magnitude between the first and second pulse shows that viscoelastic and dispersion effects are significant. The close correlation between the corrected pulse and second measured pulse demonstrate that the correction method is accurate.

To measure the timing of the color change (and thus onset of molecular bond breakage) in the mechanophore-embedded PDMS, a Photron SA-5 high-speed color camera was used to record high-speed photography of each test at a frame rate of 100,000 fps and a resolution of 256 × 512 pixels. The camera was synced to the strain gauge data using a common trigger of a laser and photodiode pair activated by the projectile. Lighting was provided by a Multiled LT-V9-15 LED backlight to ensure constant illumination throughout the duration of the experiment. The onset of color change was determined through computer image analysis of the high-speed photography, detailed in the following section.

5. New Experimental Protocol to Determine the Onset of Molecular Damage

The onset of molecular bond breakage coincides with continuum-scale color change in the bulk PDMS. However, visual identification of the onset of color change is inherently subjective. A MATLAB protocol using the Image Analysis toolbox was developed to provide an objective determination of the onset of color change. Nearest neighbor image segmentation is used to track a region of interest in the sample while excluding the bar faces and background of the image and the change in the pixel color values used to determine a quantitative threshold for the onset of color change and associated molecular damage.

To analyze an experiment and determine the timing of the color change, each image is loaded sequentially and converted into CIELAB color space.[34] This offers the advantage of separating illumination into a separate channel, minimizing the impact of decreased illumination due to the moving bars, and changing shape of the sample. A predefined mask of triangular polygons (as shown in Fig. 9) is used to specify three regions of interest: one for the bars, one for the background, and one for the sample. The mean pixel value for each color channel in each region is calculated and used to determine the "average" color of each region. Every pixel in every image is compared to the three regions and segmented based on the closest match. As the bar and background maintain a consistent color, the sample is consistently identified through this method even after the color change begins.

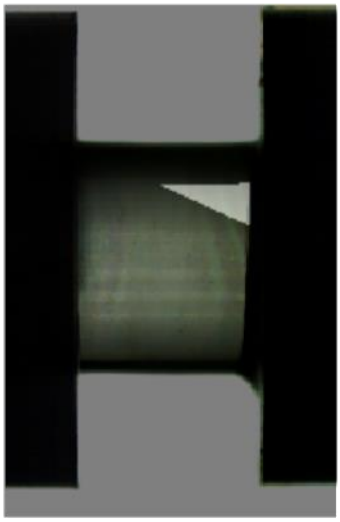

Fig. 9 An image of the sample is shown, along with a transparent overlay indicating the area used as a mask to determine the initial average sample color, used as part of the nearest neighbor segmentation to determine the sample region

Once an image has been segmented into bar, background, and sample regions using this method, the mean value of each color channel for the sample region is calculated and recorded. In this study, the blue-orange channel was found to be most effective in determining onset of color change when examined over time from beginning to end. To identify the onset of color change, the mean pixel value in the blue-orange channel is normalized by the maximum value over the course of the experiment, with 5% of the maximum value used as a threshold. The first image frame in which this threshold is crossed is the critical frame at which color change begins. Figure 10 shows a plot of the mean pixel value in the blue-orange channel over time, as well as the critical frame (marked with a circle). To confirm the validity of this method, the onset time of several samples was determined by eye prior to determination of onset using the image analysis method. All were found to agree within one frame (10 μs).

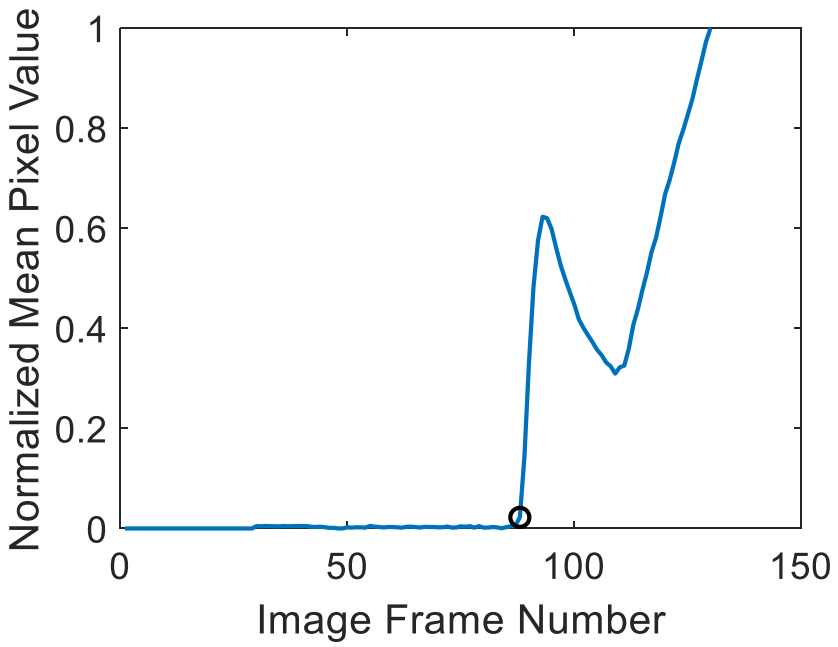

Fig. 10 The normalized mean pixel value of the blue-orange channel in the sample region is shown over the course of a typical test. The critical frame at which color change begins, Frame 88, is marked with a black circle. Frame 88 corresponds to a time of 1370 μs after the impact of the projectile onto the incident bar.

6. Results

The objective of this report is primarily to introduce a new experimental protocol depicting the onset of molecular-level bond breakage prior to macroscopic damage during a standard high-rate material characterization experiment. Four control samples of silicone elastomer (synthesized per Scheme 2 shown in Fig. 4) and seven samples using functionalized spiropyran mechanophore 1 (Fig. 3, Scheme 1) embedded into silicon elastomers were tested. The initiation of color change in the mechanophore-embedded samples was determined using the method described in Section 4. Table 1 lists the average peak stress and strain for each type of sample, as well as the average critical stress and strain at the initiation of color change for the mechanophore-embedded samples.

Table 1 Peak stress and strain and critical stress and strain at onset of color change are shown for the studied samples. Error ranges represent 1 standard deviation.

Sample type	Peak stress (MPa)	Peak strain	Strain rate	Critical stress (MPa)	Critical strain
Control	16.0 ± 0.5	0.8 ± 0.06	2000	N/A	N/A
Mechanophore	16.8 ± 1.3	0.8 ± 0.03	2200	11.7 ± 1.7	0.65 ± 0.04

There was no significant difference between the peak stress and strain in the control samples (compound **12**, see Fig. 4, Scheme 2) and the functionalized spiropyran **1** (see Figs. 2 and 3) embedded samples, demonstrating that material properties were not altered for the two configurations tested (Fig. 11). It should be noted that silicone elastomers have been shown in the literature to be dependent on curing temperature; in this study the curing temperature was the same for both cases.[35]The onset of color change occurred at approximately 75% of the peak stress and 87% of the peak strain. The variation in the timing of the color change was low. The standard deviation in the critical stress and strain is very similar to the standard deviation in the peak stress and strain measurements, suggesting that the cause of variability is present in both cases and thus not a result of the color change detection method.

Figure 12 shows a typical test of the mechanophore-embedded sample in deformed state prior to the onset of mechanophore activation along with the true stress-strain and true stress-time data marking the critical onset of mechanophore activation prior to reaching peak stress. The stress-strain curve is notably nonlinear, with the effective modulus increasing with increasing stress and strain. Barreling is significant due to the nature of the sample, despite efforts to reduce interface friction using mineral oil lubricant.

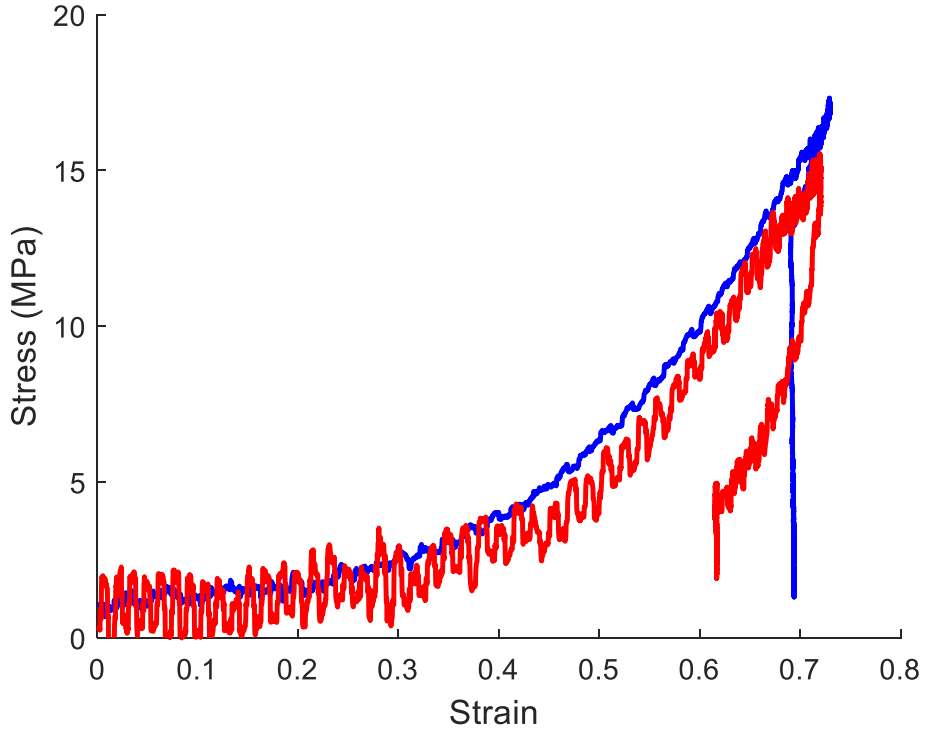

Fig. 11 Typical stress-strain curves for control (red) and functionalized (blue) spiropyran samples. The covalent embedding of a functionalized mechanophore results in no significant difference in mechanical properties.

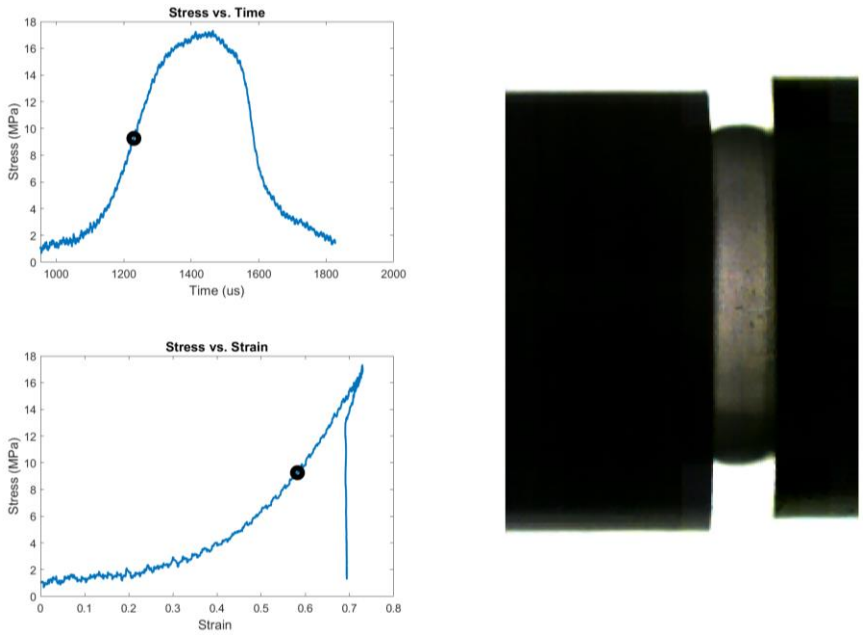

Fig. 12 (Top left) A stress-time plot of a typical test of the functionalized mechanophore 1 embedded silicone elastomer sample. The black dot marks the critical time of onset of color change. (Bottom left) A typical stress-strain plot of a mechanophore-embedded silicone elastomer sample. The black dot marks the critical stress and strain at onset of color change. (Right) The high-speed color photograph prior to the onset of color change.

Figure 13 shows the evolution of the same experiment over time. A notable contrast between the light yellow color (spiropyran) of the sample prior to activation and the blue color (merocyanine) of the post-activation sample can be seen. The color change due to mechanophore activation is observed to begin around 1370 μs after the impact of the projectile onto the incident bar. The blue color remains as the sample starts to return to its original shape as seen in Fig. 13d; however, the blue color reverts back to the original yellow color shortly after. Therefore after the impact event, the open chain merocyanine reverts back to the closed spiropyran form. The sample returns to its original color, shape and dimensions.

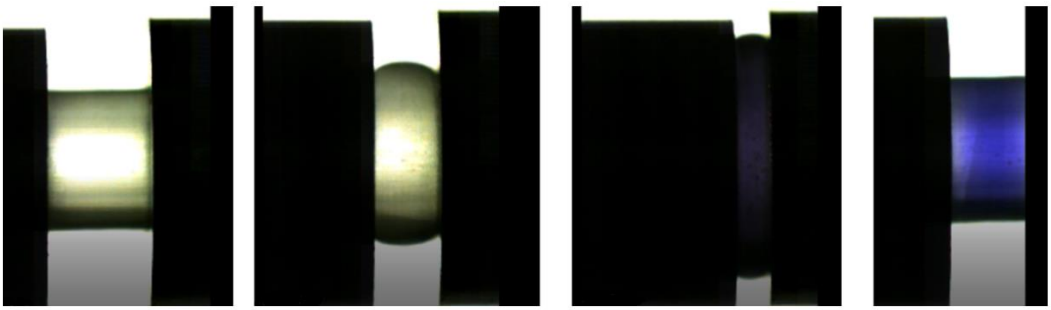

(a) 0 μs **(b) 1100 μs** **(c) 1370 μs** **(d) 2500 μs**

Fig. 13 Selected still frames from a typical experiment on the spiropyran mechanophore 1 embedded silicone elastomer

7. Summary and Conclusions

In this report, incorporation of mechanophore-embedded materials into high-rate material characterization experiments to determine the critical stress and strain for the onset of molecular-level bond breakage prior to onset of continuum-level damage is explored. Description of the new protocol, and the post-processing method to objectively detect the onset of mechanophore activation that marks the molecular-level bond breakage are provided. The schemes for the synthesis of the control spiropyran **12** and active spiropyran mechanophore **1** used in this study are included. The control group is designed such that the onset of activation in spiropyran **1** samples (see Fig. 2) is due to mechanical loading and not due to local thermal effects. It is found that the peak stress did not change between the control group, spiropyran **12**, and active spiropyran **1** embedded silicon elastomer (PDMS) samples. An image of the activated state after the sample reverts back to its original shape is included. Further studies will include differing attachment configurations of the mechanophore to the polymer backbone, and the impact of attachment location on macroscopic measurements. Data collection will continue to link molecular-level damage to macroscopic constitutive behavior and macroscopic failure (evolution of macroscopic damage), as well as tailoring the mechanophore activation for stress reporting and altering macroscopic material response in other Army-relevant materials.

8. References

1. Beyer M, Clausen-Schaumann H. Mechanochemistry: the mechanical activation of covalent bonds. Chem Rev. 2005;105(8):2921–2948.

2. Diesendruck CE, Moore JS. Mechanophores for self-healing applications. In: Binder WH, editor. Self-healing polymers: from principles to applications. Weinheim (Germany): Wiley-VCH Verlag GmbH & Co; 2013.

3. Gossweiler GR, Brown, CL, Hewage, GB, Sapiro-Gheiler E, Trautman WJ, Welshofer GW, Craig SL. Mechanochemically active soft robots. ACS Appl Mater Interfaces. 2015;7(40):22431–22435.

4. Wang Q, Gossweiler GR, Craig SL, Zhao X. Cephalopod-inspired design of electro-mechano-chemically responsive elastomers for on-demand fluorescent patterning. Nat Commun. 2014;5:4899

5. Barbee MH, Mondal K, Deng JZ, Bharambe V, Neumann TV, Adams JJ, Boechler N, Dickey MD, Craig SL. Mechanochromic stretchable electronics. ACS Appl Mater Interfaces 2018;10(35):29918–29924.

6. Peterson GI, Yurtoglu M, Larsen MB, Craig SL, Ganter MA, Storti DW, Boydston AJ. Additive manufacturing of mechanochromic polycaprolactone on entry-level systems. Rapid Prototyping J. 2015;21(5):520–527.

7. Li J, Nagamani C, Moore JS. Polymer mechanochemistry: from destructive to productive. Acc Chem Res. 2015;48(8):2181–2190.

8. Caruso MM, Davis DA, Shen Q, Odom SA, Sottos NR, White SR, Moore JS. Mechanically-induced changes in polymeric materials. Chem Rev. 2009;109(11):5755–5798.

9. Hickenboth CR, Moore JS, White SR, Sottos NR, Baudry J, Wilson SR. Biasing reaction pathways with mechanical force. Nature. 2007;446:423–427.

10. Li M, Zhang Q, Zhou Y-N, Zhu S. Let spiropyran help polymers feel force! Prog Polym Sci. 2018;79:26–39.

11. Ramirez ALB, Kean ZS, Orlicki JA, Champhekar M, Elsakr SM, Krause WE, Craig SL. Mechanochemical strengthening of a synthetic polymer in response to typically destructive shear forces. Nat Chem. 2013;5(9):757–761.

12. Larsen MB, Boydston AJ. Flex-activated mechanophores: using polymer mechanochemistry to direct bond bending activation. J Am Chem Soc. 2013;135(22):8189–8192.

13. Gossweiler GR, Hewage GB, Soriano G, Wang Q, Welshofer GW, Zhao X, Craig SL. Mechanochemical activation of covalent bonds in polymers with full and repeatable macroscopic shape recovery. ACS Macro Lett. 2014;3(3):216–219.

14. Nagamani C, Liu H, Moore JS. Mechanogeneration of acid from oxime sulfonates. J Am Chem Soc. 2016;138(8):2540–2543.

15. Piermattei A, Karthikeyan S, Sijbesma RP. Activating catalysts with mechanical force. Nat Chem. 2009;1:133–137

16. Celestine AN, Beiermann BA, Davis DA, Moore JS, Sottos NR, White SR. Fracture behavior of mechanophore-linked glassy polymers. Society of Engineering Science 47th Annual Meeting; Iowa; 2010 Oct 4–6.

17. Grady ME, Beiermann BA, Moore JS, Sottos NR. Shockwave loading of mechanochemically active polymer coatings. ACS Appl Mater Interfaces 2014;6(8):5350–5355.

18. Kingsbury CM, Davis DA, Sottos NR, White SR, Moore JS. Shear activation of mechanophore-linked PMMA. Society of Engineering Science 47th Annual Meeting; Iowa; 2010 Oct 4–6.

19. Hemmer JR, Smith PD, van Horn M, Alnemrat S, Mason BP, de Alaniz JR, Osswald S, Hooper JP. High strain-rate response of spiropyran mechanophores in PMMA. J Polym Sci Polym Phys. 2014 Aug;52(20):1347–1356.

20. Klajn R. Spiropyran-based dynamic materials. Chem Soc Rev. 2014;43(1):148–184.

21. For the first example of a spiropyran being used as a mechanophore in solution, see Potisek SL, Davis DA, Sottos NR, White SR, Moore JS. Mechanophore-linked addition polymers. J Am Chem Soc. 2007;129(45):13808–13809.

22. Kean ZS, Gossweiler GR, Kouznetsova TB, Craig SL. A coumarin dimer probe of mechanochemical scission efficiency in the sonochemical activation of chain-centered mechanophore polymers. Chem Comm. 2015;51(44):9157–9160.

23. Imato K, Kanehara T, Ohishi T, Nishihara M, Yajima H, Ito M, Takahara A, Otsuka H. Mechanochromic dynamic covalent elastomers:quantitative stress evaluation and autonomous recovery. ACS Macro. Lett. 2015;4(11):1307–1311. Imato K, Otsuka H. Reorganizable and stimuli-responsive polymers based on dynamic carbon–carbon linkages in diarylbibenzofuranones. Polymer. 2018;137:395–413.

24. Robb MJ, Kim TA, Halmes AJ, White SR, Sottos NR, Moore JS. Regioisomer-specific mechanochromism of naphthopyran in polymeric materials. J Am Chem Soc. 2016;138(38):12328–12331.

25. Sagara Y, Karman M, Verde-Sesto E, Matsuo K, Kim Y, Tamaoki N, Weder C. Rotaxanes as mechanochromic fluorescent force transducers in polymers. J Am Chem Soc. 2018;140(5):1584–1587.

26. Di Giannantonio M, Ayer MA, Verde-Sesto E, Lattuada M, Weder C, Fromm KM. Triggered metal ion release and oxidation: ferrocene as a mechanophore in polymers. Angew Chem Int Ed. 2018;57(35):11445–11450.

27. Sha Y, Zhang Y, Xu E, Wang Z, Zhu T, Craig SL, Tang C. Quantitative and mechanistic mechanochemistry in ferrocene dissociation. ACS Macro Lett. 2018;7:1174–1179.

28. Lenhardt JM, Black AL, Beiermann BA, Steinberg B, Rahman F, Samborski T, Elsakr J, Moore JS, Sottos NR, Craig SL. Characterizing the mechanochemically active domains in gem-dihalocyclopropanated polybutadiene under compression and tension. J Mater Chem. 2011;21(23):8454–8459.

29. Davis DA, Hamilton A, Yang J, Cremar LD, Van Gough D, Potisek SL, Ong MT, Braun PV, Martinez TJ, White SR, et al. Force induced activation of covalent bonds in mechanoresponsive polymeric materials. Nature 2009;459:68–72.

30. Achard TRJ, Clegg W, Harrington RW, North M. Chiral salen ligands designed to form polymetallic complexes. Tetrahedron 2012;68(1):133-144.

31. Gossweiler GR, Kouznetsova TB, Craig SL. Force rate characterization of two spiropyran-based molecular force probes. J Am Chem Soc. 2015;137(19): 6148–6151.

32. Chen WW, Song B. Split Hopkinson (Kolsky) bar: design, testing and applications. Springer Science & Business Media; 2010.

33. Bacon C. An experimental method for considering dispersion and attenuation in a viscoelastic Hopkinson bar. Experimental mechanics. 1998;38(4):242–249.

34. International Commission on Illumination (CIE). Official recommendations on uniform color spaces, color-difference equations, and metric color terms. Vienna (Austria): CIE; 1978. CIE Publication No. 15, Supplement Number 2 (E-1.3. 1, 1971).

35. Johnston ID, McCluskey DK, Tan CKL, Tracey MC. Mechanical characterization of bulk Sylgard 184 for microfluidics and microengineering. Journal of Micromechanics and Microengineering. 2014;24(3):035017.

Appendix. Experimental Methods

Most solvents were purchased from either Sigma-Aldrich or VWR International and used as is, except tetrahydrofuran (THF), which was dried on an MBraun, Inc., Solvent Purification System prior to use. Absolute ethanol was purchased from Koptec, Inc., and petroleum ether was purchased from GFS Chemicals, Inc. $CDCl_3$ was purchased from Sigma-Aldrich, and DMSO-d_6 was purchased from Cambridge Isotope Laboratories. Sylgard-184 silicone elastomer kit was purchased from Krayden, Inc. All other reagents were purchased from either Sigma-Aldrich or Alfa Aesar. All glassware was dried in an oven set to 110 °C, and reactions were stirred magnetically under an argon atmosphere. Thin layer chromatography (TLC) was performed using EMD/Millipore Silica Gel 60 TLC plates (250 µm, F_{254} indicator) and viewed under UV light (254 nm). Column chromatography was performed using SiliCycle SiliaFlash F60 silica gel (40- to 63-µm particle size, 230–400 mesh). ^{1}H-NMR and ^{13}C-NMR were performed on a Bruker 400-MHz nuclear magnetic resonance (NMR) system. NMR values are reported in parts per million (ppm) as compared to the reference peaks of $CDCl_3$ (7.26 ppm for ^{1}H and 77.16 ppm for ^{13}C) and DMSO-d_6 (2.50 ppm for ^{1}H and 39.52 ppm for ^{13}C). ^{1}H-NMR values are reported as (chemical shift in parts per million, multiplicity, coupling constant in hertz, relative integral). ^{1}H-NMR multiplicities are indicated as s (singlet), d (doublet), t (triplet), dd (doublet of doublets), td (triplet of doublets), m (multiplet), and b (broad). EtOH is ethanol, EtOAc is ethyl acetate, DCM is dichloromethane, Et_2O is diethyl ether, THF is tetrahydrofuran, MeOH is methanol, PE is petroleum ether, HBr is hydrobromic acid, $NaHCO_3$ is sodium bicarbonate, $MgSO_4$ is magnesium sulfate, and PDMS is polydimethylsiloxane.

1-(2-hydroxyethyl)-2,3,3-trimethyl-3*H*-indolium iodide (3)

Following a modified literature procedure [1], 2-iodoethanol (7.36 mL, 94.3 mmol, 1.5 equiv.) was added dropwise over 5 min to a solution of 2,3,3-trimethyl-3*H*-indole **2** (10.0 g, 62.9 mmol, 1 equiv.) in 100 mL of toluene. The mixture was heated to reflux (bath temperature 120 °C) and stirred for 20 h. After cooling to room temperature, the mixture was further cooled to 0 °C in an ice bath, then filtered to give a dark purple solid, which was washed with ice cold toluene. The solid was triturated several times with acetone to give 1-(2-hydroxyethyl)-2,3,3-trimethyl-3*H*-indolium iodide **3** (17.08 g, 82% yield) as a light pink solid. ^{1}H-NMR and ^{13}C-NMR were in agreement with the previously reported material [1]. ^{1}H-NMR (400 MHz, DMSO-d_6) δ 7.97-7.94 (m, 1H), 7.86-7.84 (m, 1H), 7.64-7.60 (m, 2H), 4.60 (t, J = 5.0 Hz, 2H), 3.88 (t, J = 5.0 Hz, 2H), 2.82 (s, 3H), 1.55 (s, 6H). ^{13}C-NMR (100 MHz, DMSO-d_6) δ 197.8, 141.8, 141.1, 129.3, 128.8, 123.4, 115.6, 57.8, 54.2, 50.2, 22.0, 14.4.

2-(7-(hydroxymethyl)-3',3'-dimethylspiro[chromene-2,2'-indolin]-1'-yl)ethan-1-ol (5)

Following a modified literature procedure [1], piperidine (0.39 mL, 4 mmol, 2 equiv.) was added to a stirring solution of 1-(2-hydroxyethyl)-2,3,3-trimethyl-3*H*-indolium iodide **3** (0.66 g, 2.00 mmol, 1 equiv.) and 2-hydroxy-4-(hydroxymethyl)benzaldehyde **4** [2] (0.30 g, 2.00 mmol, 1 equiv.) in 10 mL of absolute EtOH. The solution was refluxed overnight and, after cooling to room temperature, was concentrated under reduced pressure to give a brown oil. This oil was then dissolved in 100 mL of EtOAc, washed with 100 mL of water (x3), 100 mL of brine (x1), and then the organic phase was dried with $MgSO_4$. Solvent removal via rotary evaporation afforded 2-(7-(hydroxymethyl)-3',3'-dimethylspiro[chromene-2,2'-indolin]-1'-yl)ethan-1-ol **5** (658 mg, 88% yield) as a light brown foam. ^{1}H NMR (400 MHz, $CDCl_3$) δ 7.16 (td, *J* = 7.7, 1.4 Hz, 1H), 7.08 (dd, *J* = 7.3, 1.3 Hz, 1H), 7.03 (d, *J* = 7.6 Hz, 1H), 6.91 – 6.79 (m, 3H), 6.71 (d, *J* = 1.5 Hz, 1H), 6.63 (d, *J* = 7.7 Hz, 1H), 5.67 (d, *J* = 10.3 Hz, 1H), 4.57 (s, 2H), 3.74 (m, 4H), 3.50 (m, 1H), 3.33 (m, 1H), 1.30 (s, 3H), 1.17 (s, 3H). ^{13}C NMR (125 MHz, $CDCl_3$) δ 153.9, 147.3, 143.3, 136.4, 129.2, 127.6, 127.0, 121.8, 119.4, 119.3, 118.9, 117.8, 113.3, 106.6, 104.7, 64.6, 60.7, 52.3, 45.9, 25.9, 20.4.

(1'-(2-(hept-6-enoyloxy)ethyl)-3',3'-dimethylspiro[chromene-2,2'-indolin]-7-yl)methyl hept-6-enoate (1)

To a solution of 2-(7-(hydroxymethyl)-3',3'-dimethylspiro[chromene-2,2'-indolin]-1'-yl)ethan-1-ol **5** (0.5 g, 1.48 mmol, 1 equiv.) in 12-mL dry THF was added hept-6-enoic anhydride [1] (0.74 g, 3.11 mmol, 2.1 equiv.) and 4-dimethylaminopyridine (DMAP) (0.018 g, 0.148 mmol, 0.1 equiv.). The solution was stirred at room temperature overnight, then 0.5 mL NEt_3 was added to the solution and it was stirred for an additional 30 min. Solvent removal under reduced pressure, followed by column chromatography (0% to 25% EtOAc/hexane gradient eluent), gave (1'-(2-(hept-6-enoyloxy)ethyl)-3',3'-dimethylspiro[chromene-2,2'-indolin]-7-yl) methyl hept-6-enoate **1** (704 mg, 85% yield) as a light orange oil. ^{1}H NMR (400 MHz, $CDCl_3$) δ 7.17 (t, *J* = 7.6 Hz, 1H), 7.07 (d, *J* = 7.1 Hz, 1H), 7.02 (d, *J* = 7.7 Hz, 1H), 6.92 – 6.73 (m, 3H), 6.73 – 6.61 (m, 2H), 5.77 (m, 2H), 5.70 (d, *J* = 10.2 Hz, 1H), 4.98 (s, 2H), 4.97 – 4.90 (m, 4H), 4.25 (dt, *J* = 11.0, 6.4 Hz, 1H), 4.16 (dt, *J* = 11.5, 6.3 Hz, 1H), 3.51 (m, 1H), 3.38 – 3.29 (m, 1H), 2.34 (t, *J* = 7.5 Hz, 2H), 2.26 (t, *J* = 7.5 Hz, 2H), 2.03 (p, *J* = 7.3 Hz, 4H), 1.62 (m, 4H), 1.39 (m, 4H), 1.28 (s, 3H), 1.14 (s, 3H). ^{13}C NMR (126 MHz, $CDCl_3$) δ 173.6, 173.5, 154.3, 147.3, 138.5, 138.2, 136.3, 129.2, 127.7, 127.0, 121.8, 119.8, 119.6, 119.4, 118.3, 114.8, 114.4, 106.6, 104.7, 65.7, 62.8, 52.4, 42.6, 34.2, 34.1, 33.4, 28.4, 26.0, 24.5, 24.4, 20.1.

5-methoxy-2,3,3-trimethyl-3*H*-indole (7)

Following the literature procedure [3], 4-methoxyphenylhydrazine hydrochloride **6** (5.00 g, 28.7 mmol, 1 equiv.) was stirred in 133-mL absolute EtOH, and methyl isopropyl ketone (3.07 mL, 28.7 mmol, 1 equiv.) was added. The mixture was then refluxed overnight in an oil bath set to 100 °C. After cooling and removing the solvent, the product was purified via column chromatography (product R_f = 0.14 in 3:1 hexane:EtOAc) to give 5-methoxy-2,3,3-trimethyl-3*H*-indole **7** (4.57 g, 84% yield) as a red oil that solidified upon standing. ^{1}H-NMR and ^{13}C-NMR were in agreement with the previously reported material [3]. ^{1}H-NMR (400 MHz, $CDCl_3$) δ 7.41 (d, *J* = 8.2 Hz, 1H), 6.84-6.78 (m, 2H), 3.81 (s, 3H), 2.23 (s, 3H), 1.27 (s, 6H). ^{13}C-NMR (100 MHz, $CDCl_3$) δ 185.8, 158.0, 147.6, 147.4, 120.2, 112.1, 108.2, 55.8, 53.9, 23.3, 15.4.

2,3,3-trimethyl-3*H*-indol-5-ol (8)

Following the literature procedure [4], 5-methoxy-2,3,3-trimethyl-3*H*-indole **7** (4.50 g, 23.8 mmol, 1 equiv.) was stirred with 90 mL of 48% aq. HBr and heated to reflux (bath temperature 140 °C) for 5 h. After cooling to room temperature, the mixture was slowly diluted with 300 mL of water and then solid $NaHCO_3$ was slowly added in small portions with vigorous stirring until the reaction became basic and the evolution of gas stopped. The solid product was filtered and washed with water. The filtrate was extracted three times with DCM and after removal of the solvent, the solids were combined to give 2,3,3-trimethyl-3*H*-indol-5-ol **8** (4.01 g, 96% yield) as a light brown powder that was used without further purification. ^{1}H-NMR (400 MHz, $CDCl_3$) δ 8.93 (bs, 1H), 7.31 (d, *J* = 7.8 Hz, 1H), 6.84 (d, *J* = 2.4 Hz, 1H), 6.77 (dd, *J* = 8.2, 2.4 Hz, 1H), 2.26 (s, 3H), 1.28 (s, 6H). ^{13}C-NMR (100 MHz, $CDCl_3$) δ 185.9, 155.6, 147.5, 145.5, 120.1, 114.3, 109.9, 53.8, 23.3, 15.1.

5-hydroxy-1-(2-hydroxyethyl)-2,3,3-trimethyl-3H-indol-1-ium iodide (9)

Following the literature procedure [1], 2,3,3-trimethyl-3*H*-indol-5-ol **8** (9.01 g, 51.4 mmol, 1 equiv.) and 2-iodoethanol (6.0 mL, 77.2 mmol, 1.5 equiv.) were added to 75 mL of toluene and heated to reflux for 12 h (bath temperature 120 °C). After cooling, the mixture was placed in the refrigerator overnight, then the solid was collected and rinsed with cold EtOH to give 5-hydroxy-1-(2-hydroxyethyl)-2,3,3-trimethyl-3*H*-indol-1-ium iodide **9** (12.56 g, 71% yield) as a brown solid that was used without further purification. ^{1}H NMR (400 MHz, DMSO) δ 10.25 (s, 1H), 7.72 (d, *J* = 8.8 Hz, 1H), 7.15 (d, *J* = 2.4 Hz, 1H), 6.93 (dd, *J* = 8.8, 2.4 Hz, 1H), 4.51 (t, *J* = 5.0 Hz, 2H), 3.84 (t, *J* = 5.0 Hz, 2H), 2.73 (s, 3H), 1.49 (s, 3H). ^{13}C-

NMR (100 MHz, DMSO) δ 193.5, 159.0, 144.0, 133.0, 116.5, 115.1, 110.4, 57.8, 53.7, 50.2, 22.2, 14.0.

1'-(2-hydroxyethyl)-3',3'-dimethyl-6-nitrospiro[chromene-2,2'-indolin]-5'-ol (11)

Following a slightly modified literature procedure [4], 5-hydroxy-1-(2-hydroxyethyl)-2,3,3-trimethyl-3*H*-indol-1-ium iodide **9** (12.56 g, 36.2 mmol, 1 equiv.) and commercially available 2-hydroxy-5-nitrobenzaldehyde **10** (6.05 g, 36.2 mmol, 1 equiv.) were dissolved in 400 mL of absolute EtOH. Piperidine (3.73 mL, 36.2 mmol, 1 equiv.) was added and the reaction was heated to 85 °C for 12 h. The reaction was concentrated to half the original volume and stored in the refrigerator to precipitate the solid product. The solids were collection by vacuum filtration and rinsed with cold ethanol to give 1'-(2-hydroxyethyl)-3',3'-dimethyl-6-nitrospiro[chromene-2,2'-indolin]-5'-ol **11** (12.49 g, 94% yield) as a dark purple solid. This material was used directly without purification.

3',3'-dimethyl-6-nitro-1'-(2-(pent-4-enoyloxy)ethyl)spiro[chromene-2,2'-indolin]-5'-yl pent-4-enoate (12)

Following the literature procedure [1], 1'-(2-hydroxyethyl)-3',3'-dimethyl-6-nitrospiro[chromene-2,2'-indolin]-5'-ol **11** (6.00 g, 16.3 mmol, 1 equiv.) and 4-dimethylaminopyridine (0.99 g, 8.14 mmol, 0.5 equiv.) were dissolved in 215 mL of DCM. 4-pentenoic anhydride (6.25 mL, 34.2 mmol, 2.1 equiv.) was added dropwise, and the reaction was stirred at room temperature for 24 h. The reaction mixture was concentrated to half its volume and filtered through a plug of basic alumina, eluting with DCM. The solution was washed with water three times, followed by brine. After drying over sodium sulfate, the solution was concentrated to give 3',3'-dimethyl-6-nitro-1'-(2-(pent-4-enoyloxy)ethyl)spiro[chromene-2,2'-indolin]-5'-yl pent-4-enoate **12** (5.18 g, 60% yield) as a yellow oil. ^{1}H NMR (400 MHz, $CDCl_3$) δ 8.03 (dd, *J* = 8.9, 2.7 Hz, 1H), 8.00 (d, *J* = 2.7 Hz, 1H), 6.92 (s, 1H), 6.87 (dd, *J* = 8.3, 2.3 Hz, 1H), 6.80 (d, *J* = 2.3 Hz, 1H), 6.77 (d, *J* = 8.9 Hz, 1H), 6.63 (d, *J* = 8.4 Hz, 1H), 5.86 (d, *J* = 10.3 Hz, 1H), 5.97 – 5.70 (m, 3H), 5.19 – 4.93 (m, 4H), 4.32 – 4.09 (m, 2H), 3.53 – 3.30 (m, 2H), 2.66 (t, *J* = 7.4 Hz, 2H), 2.51 (q, *J* = 6.8 Hz, 2H), 2.34 (q, *J* = 5.9, 5.4 Hz, 4H), 1.24 (s, 3H), 1.16 (s, 3H). ^{13}C NMR (126 MHz, $CDCl_3$) δ 172.9, 172.2, 159.3, 144.5, 144.3, 141.2, 136.9, 136.5, 128.5, 126.1, 122.8, 121.5, 120.3, 118.4, 115.9, 115.8, 115.7, 115.6, 106.8, 62.4, 60.4, 52.9, 42.6, 33.7, 33.4, 29.0, 28.8, 25.8, 19.8, 14.3.

PDMS Curing Procedure

Slygard-184 silicone elastomer was used as the PDMS bulk material for testing. Typically, a 10:1 ratio of elastomer base:curing agent was used. A representative procedure is as follows: 7.00 g of silicone elastomer base was weighed into a 40-mL scintillation vial. Separately, 38.5 mg (0.5% by total weight) functionalized spiropyran mechanophore was dissolved in 0.5 mL xylenes in a small vial. The mechanophore solution was then added to the elastomer base and vortexed for 2 min to ensure complete mixing. Next, 0.7 g of curing agent was added to the elastomer/mechanophore mixture and vortexed for 2 min to ensure complete mixing. This mixture was then poured into the cavities of the aluminum mold, and the entire mold was placed under vacuum for 1 h to remove air bubbles. After releasing the vacuum, followed by removal from the oven, a large plastic pipette was used to pop all of the remaining air bubbles that traveled to the surface. The entire mold was then placed into an oven and cured at 68 °C for 24 h. After removal from the oven, the mold was allowed to cool to room temperature, and the screws were removed from the outside of the mold. A small metal spatula was then used to help dislodge the top of the sample from the lip of the mold. The bottom piece of the mold was removed, followed by careful separation of the side components to prevent tearing of the sample. The samples were then carefully pulled from the top portion of the mold. Using this procedure, six cylinders were produced, which were then cut into smaller dimensions to obtain 18 to 24 samples from each curing event.

Appendix References

1. Gossweiler GR, Hewage GB, Soriano G, Wang Q, Welshofer GW, Zhao X, Craig SL. Mechanochemical activation of covalent bonds in polymers with full and repeatable macroscopic shape recovery. ACS Macro Lett. 2014;3(3):216–219.

2. Achard TRJ, Clegg W, Harrington RW, North M. Chiral salen ligands designed to form polymetallic complexes. Tetrahedron 2012;68(1):133-144.

3. Potisek SL, Davis DA, Sottos NR, White SR, Moore JS. Mechanophore-linked addition polymers. J Am Chem Soc. 2007;129(45):13808–13809.

4. Davis DA, Hamilton A, Yang J, Cremar LD, Van Gough D, Potisek SL, Ong MT, Braun PV, Martinez TJ, White SR, et al. Force induced activation of covalent bonds in mechanoresponsive polymeric materials. Nature 2009;459:68–72.

List of Symbols, Abbreviations, and Acronyms

1-D	one-dimensional
3-D	three-dimensional
DCM	dichloromethane
DMAP	4-dimethylaminopyridine
Et_2O	diethyl ether
EtOH	ethanol
EtOAc	ethyl acetate
HBr	hydrobromic acid
LED	light-emitting diode
MeOH	methanol
$MgSO_4$	magnesium sulfate
$NaHCO_3$	sodium bicarbonate
NMR	nuclear magnetic resonance
PDMS	polydimethylsiloxane
PE	petroleum ether
PMA	poly(methyl acrylate)
PMMA	poly(methyl methacrylate)
SHPB	split Hopkinson pressure bar
SP	spiropyran
THF	tetrahydrofuran
TLC	thin layer chromatography
UV	ultraviolet

1 (PDF) DEFENSE TECHNICAL INFORMATION CTR
DTIC OCA

2 (PDF) DIR ARL
IMAL HRA
RECORDS MGMT
RDRL DCL
TECH LIB

1 (PDF) GOVT PRINTG OFC
A MALHOTRA

1 (PDF) AFRL
D LAMBERT

1 (PDF) APPLIED PHYSICS LABORATORY
Z XIA

2 (PDF) NATICK SOLDIER RES DEV ENG CTR
S FILOCAMO
C DOONA

3 (PDF) DUKE UNIVERSITY
S CRAIG
M BARBEE
Y LIN

26 (PDF, HC) ARL
RDRL D
P PERCONTI
RDRL WM
J ZABINSKI
S KARNA
S SCHOENFELD
A RAWLETT
J CIEZAK-JENKINS
RDRL WMM
M VANLANDINGHAM
RDRL WMM A
R LAMBETH
T PLAISTED
E WETZEL
RDRL WMM G
J LENHART
J ORLICKI
RDRL WML
T SHEPPARD
RDRL WMP
D LYON
RDRL WMP B
C HOPPEL
S SATAPATHY
RDRL WMP C
R BECKER
J BERRY
D CASEM
M FERMEN-COKER
L SHANNAHAN
C WILLIAMS
J CLAYTON
RDRL VT
J RIDDICK
RDRL VTM
D COLE
A HALL